

A. Colliander, L. Ruokokoski, J. Suomela, K. Veijola, J. Kettunen, V. Kangas, A. Aalto, M. Levander, H. Greus, M. T. Hallikainen, J. Lahtinen, Development and Calibration of SMOS Reference Radiometer, *IEEE Transactions on Geoscience and Remote Sensing*, vol. 45, no. 7, pp. 1967-1977, July 2007.

© 2007 IEEE

Reprinted with permission.

This material is posted here with permission of the IEEE. Such permission of the IEEE does not in any way imply IEEE endorsement of any of Helsinki University of Technology's products or services. Internal or personal use of this material is permitted. However, permission to reprint/republish this material for advertising or promotional purposes or for creating new collective works for resale or redistribution must be obtained from the IEEE by writing to [pubs-permissions@ieee.org](mailto:pubs-permissions@ieee.org).

By choosing to view this document, you agree to all provisions of the copyright laws protecting it.

# Development and Calibration of SMOS Reference Radiometer

Andreas Colliander, *Associate Member, IEEE*, Lasse Ruokokoski, Jani Suomela, Katriina Veijola, Jani Kettunen, Ville Kangas, Alekski Aalto, Mikael Levander, Heli Greus, Martti T. Hallikainen, *Fellow, IEEE*, and Janne Lahtinen, *Member, IEEE*

**Abstract**—Three flight models (FMs) of the reference radiometer of the Soil Moisture and Ocean Salinity (SMOS) mission have been developed and tested. SMOS is a joint mission of the European Space Agency, Centre National d'Etudes Spatiales of France, and Centre for the Development of Industrial Technology of Spain. The reference radiometer is a noise injection radiometer (NIR); the NIR subsystem FM has been developed by Elektrobit Microwave, Ltd., in collaboration with the Laboratory of Space Technology of Helsinki University of Technology, which has acted as a subcontractor. The NIR subsystem will be integrated into the Microwave Imaging Radiometer Using Aperture Synthesis (MIRAS) payload in 2006. MIRAS will be the sole instrument onboard the SMOS satellite. MIRAS has 66 total power receiver units (light and cost-effective front end) and three NIR units. The purpose of the NIR subsystem is 1) to provide precise measurement of the average brightness temperature scene for absolute calibration of the MIRAS image map, 2) to measure the noise temperature level of the internal active calibration sources of MIRAS [referred to as the calibration subsystem (CAS)], and 3) to form interferometer baselines, so-called mixed baselines, with the regular receiver units. The performance of the NIR is a decisive factor of overall MIRAS performance. In this paper, we present the design solutions for the NIR FMs, which enable the achievement of the mission goals set for the NIR subsystem. The results of the NIR test campaign, proving that the performance and environmental

requirements are fulfilled, are also presented, and the outcome of the ground calibration campaign is analyzed. Furthermore, the orbital calibration scheme is depicted; the calibration scheme enables the NIR to measure its targets with precision.

**Index Terms**—Microwave Imaging Radiometer Using Aperture Synthesis (MIRAS), polarimetric radiometry, radiometry, Soil Moisture and Ocean Salinity (SMOS), synthetic aperture radiometers.

## I. INTRODUCTION

**L**-BAND REMOTE sensing radiometers can be used to measure soil moisture [1] and sea surface salinity [2]. Both of these parameters are valuable in improving weather forecasting and climate monitoring. During the past few years, there has been a great interest in radiometric measurements in the protected L-band frequency range, 1400–1427 MHz. However, to obtain sufficient spatial resolution from space, a large antenna size is required. This is difficult using conventional real-aperture antennas. Therefore, aperture synthesis by means of interferometry is an attractive option.

In this paper, three flight models (FMs) of the reference radiometer of the synthetic aperture radiometer mission Soil Moisture and Ocean Salinity (SMOS) [3] have been designed, implemented and tested. SMOS is a joint mission of the European Space Agency (ESA), Centre National d'Etudes Spatiales of France, and Centre for the Development of Industrial Technology of Spain. Due to its architecture, the reference radiometer is referred to as the noise injection radiometer (NIR). The NIR subsystem FM has been developed by Elektrobit Microwave (EBM), Ltd., in collaboration with the Laboratory of Space Technology, Helsinki University of Technology (TKK); TKK has been the main subcontractor, being responsible for the tests, calibration, and field programmable gate array (FPGA) implementation. The engineering model of NIR is presented in [4] and the prototype in [5]. The calibration program of the NIR includes ground and orbital calibration, both vital for the performance of the instrument. The ground calibration was completed in spring 2006; the results are presented here.

The NIR subsystem, which consists of these three NIR units, will work as part of the Microwave Imaging Radiometer Using Aperture Synthesis (MIRAS) instrument [6], [7]. MIRAS is the sole instrument onboard the SMOS satellite; the prime contractor of MIRAS is European Aeronautic Defence and Space Company EADS N.V. (EADS)-Construcciones Aeronáuticas SA (CASA) Espacio of Spain. The main purposes of NIR are

Manuscript received June 1, 2006; revised November 28, 2006. This work was supported in part by the European Space Agency (ESA) and in part by U. Tuominen, J. Wihuri, and A. Wihuri, W. Ahlström, and Finnish Cultural Foundations. This work was performed within the SMOS Phase CD, which is managed by EADS-CASA Espacio. EBM, Ltd., is subcontracted by EADS-CASA Espacio and TKK is acting as a subcontractor of EBM.

A. Colliander is with the Laboratory of Space Technology, Helsinki University of Technology, 02015 Espoo, Finland, and also with the European Space Research and Technology Centre, European Space Agency, 2200 AG Noordwijk, The Netherlands (e-mail: andreas.colliander@esa.int).

L. Ruokokoski was with Elektrobit Microwave, Ltd., 02700 Kauniainen, Finland. He is now with Turku School of Economics, 20500 Turku, Finland (e-mail: lasse.ruokokoski@tse.fi).

J. Suomela was with the Helsinki University of Technology, 02015 Espoo, Finland. He is now with Finavia, the Civil Aviation Administration, 01531 Vantaa, Finland (e-mail: jani.suomela@finavia.fi).

K. Veijola, A. Aalto, and M. T. Hallikainen are with the Helsinki University of Technology, 02015 Espoo, Finland (e-mail: katriina.veijola@tkk.fi; aleksi.aalto@tkk.fi; martti.hallikainen@tkk.fi).

J. Kettunen was with the Helsinki University of Technology, 02015 Espoo, Finland. He is now with Vaisala, Ltd., 00421 Helsinki, Finland (e-mail: jani.kettunen@vaisala.com).

V. Kangas and M. Levander are with Elektrobit, Ltd., 02150 Espoo, Finland (e-mail: ville.kangas@elektrobit.com; mikael.levander@elektrobit.com).

H. Greus was with Elektrobit, Ltd., 02150 Espoo, Finland. She is now with the European Space Research and Technology Centre, European Space Agency, 2200 AG Noordwijk, The Netherlands (e-mail: heli.greus@esa.int).

J. Lahtinen was with Ylinen Electronics, 02700 Kauniainen, Finland (e-mail: spaceman@elisane.fi).

Digital Object Identifier 10.1109/TGRS.2007.894055

1) to provide precise measurement of the average brightness temperature scene for the absolute calibration of the MIRAS image map, 2) to measure the noise temperature level of the internal active calibration source (the calibration subsystem (CAS), [8]) for individual receiver calibration, and 3) to form interferometer baselines with the regular receiver units in the MIRAS array (so-called mixed baselines).

In the antenna measurement mode, the NIR measures the so-called modified Stokes parameters in brightness temperature, which are defined under the Rayleigh–Jeans approximation as [9]

$$\mathbf{T} = \begin{bmatrix} T_v \\ T_h \\ T_3 \\ T_4 \end{bmatrix} \quad (1)$$

$$= \frac{\lambda^2}{k_B \eta B} \begin{bmatrix} \langle |E_v|^2 \rangle \\ \langle |E_h|^2 \rangle \\ 2\Re\{ \langle E_v E_h^* \rangle \} \\ 2\Im\{ \langle E_v E_h^* \rangle \} \end{bmatrix} \quad (2)$$

$$= \begin{bmatrix} T_v \\ T_h \\ 2\sqrt{T_v T_h} \Re\{V\} \\ 2\sqrt{T_v T_h} \Im\{V\} \end{bmatrix}$$

where  $T_v$ ,  $T_h$ ,  $T_3$ , and  $T_4$  are the brightness temperatures of the vertically and horizontally polarized radiation and third and fourth Stokes parameter, respectively;  $\lambda$  is the wavelength;  $k_B$  is Boltzmann's constant;  $\eta$  is the impedance of the medium;  $B$  is the bandwidth;  $E_v$  and  $E_h$  are the vertically and horizontally polarized electric fields, and  $V$  is the denormalized correlation between the horizontal and vertical channels. The brackets (expectation operators) stand for the infinite time average.

As the NIR will be the absolute reference for the MIRAS measurements, its performance is of paramount importance to the mission. The challenges in the measurements are the facts that there is only one accurate external target (cold sky), the individual antennas have a wide field of view, the physical temperature of the NIR is not actively stabilized, and certain calibration parameters cannot be measured in orbit, but on ground only.

In addition to the on-ground characterization, the test campaign of the NIR FM included environmental acceptance and qualification tests [vibration, thermal vacuum, and electromagnetic compatibility (EMC) tests]. One NIR unit was tested according to qualification test limits, whereas the other two were tested according to acceptance-test limits.

## II. REFERENCE RADIOMETER

The NIR has a set of requirements that are based on the SMOS mission requirements. Table I lists some of the key performance parameters. Especially noteworthy is the requirement for stability; 0.02 K/°C is a very stringent value, considering the absence of an active thermal stabilization system at subsystem level, as well as the budgetary and schedule constraints set for the development. In the following sections, the hardware of the NIR is described and the operation is discussed in detail.

TABLE I  
SOME KEY PERFORMANCE REQUIREMENTS OF NIR

Parameter	Value
Receiver noise temperature	275 K
Resolution, H and V	0.25 K
Resolution, 3 and 4	0.55 K
Stability	0.2 K/°C
Stability (with compensation)	0.02 K/°C
Channel isolation	> 40 dB

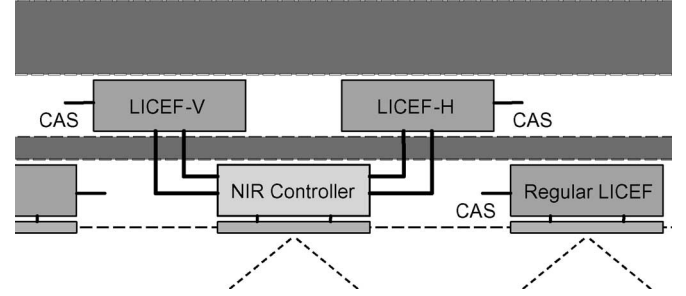


Fig. 1. Schematic diagram of an NIR unit onboard MIRAS. One NIR radiometer consists of two LICEF units, phase-stable low-loss cables, a controller, and an antenna that is identical to those in the regular LICEF-units.

### A. Hardware

An NIR FM consists of 1) two radiometer receivers, one for vertical and one for horizontal polarization, 2) a controller, and 3) four phase-stable low-loss RF cables that connect the controller to the receivers. The controller incorporates an antenna that receives the target noise. The NIR receivers, light and cost-effective front end (LICEF), are almost identical to the other receivers of MIRAS and have been manufactured by MIER Telecomunicaciones, Spain. Also, the antenna is identical to those of the other antennas of MIRAS (manufactured by RYMSA, Spain). Both antenna and receivers are provided by the main contractor as customer furnished equipment. Fig. 1 shows a schematic diagram of the placement of the NIR in the payload.

The functions of the controller are to 1) inject reference noise into the two receiver chains, 2) regulate the amount of the injected noise to keep the system balanced with antenna temperature or with the calibration noise from CAS, and 3) control the switches of NIR (Dicke switches of the receivers and the noise switches of the controller) according to the selected operation mode. A photograph of the controller is presented in Fig. 2. Due to practical reasons, the engineering model is shown; the FM looks the same. A schematic diagram of the V-channel of the NIR is presented in Fig. 3. The basic blocks of the controller are bias circuitry, which generates the required voltages and provides EMC protection (omitted in the figure), two noise injection circuitries and couplers (for vertical and horizontal polarization channels), and an FPGA circuitry, which controls the noise injection circuitry and front-end switches of the NIR receivers.

In Fig. 3, 1B/2L stands for 1-bit/2-level digital output for the correlator of MIRAS, used to retrieve the third and fourth Stokes parameters or to form correlations for mixed baselines,

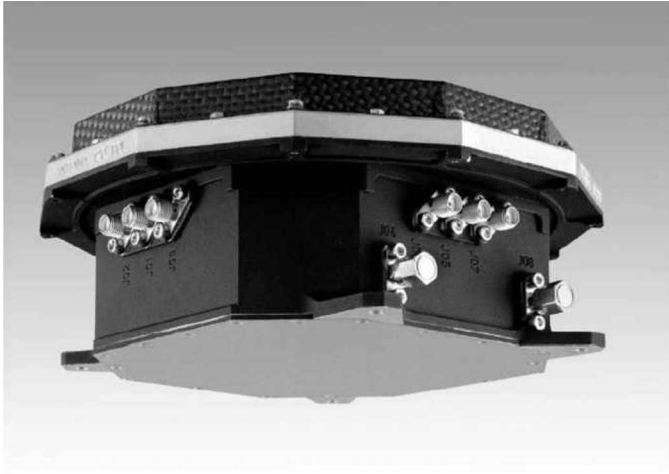


Fig. 2. Photograph of NIR controller Engineering Model; the appearance of the FM is practically identical.

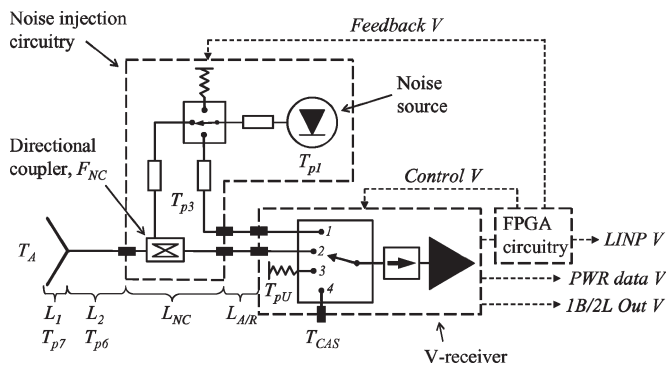


Fig. 3. Schematic diagram of the structure of the V-channel of the NIR. The H-channel is identical. In the diagram,  $L$  stands for loss,  $T_p$  for physical temperature,  $T_A$  for antenna temperature, and  $T_{CAS}$  for CAS noise temperature. The symbols are discussed in detail in relation to (6)–(19). Note that actually there are two switches in series to control the noise injection in order to improve the isolation of the switching, but in the schematic, one of the switches is excluded for clarity.

PWR is a detector signal to retrieve system temperature, and LINP stands for length of injected noise pulse to retrieve antenna temperature and the noise level of CAS. Note that there are two alternative paths for the noise injection into the receivers: one through the antenna branch for antenna temperature measurement and one to go directly to the front-end switch of the receivers. The second path is applied for the calibration of the noise level of CAS. In the receivers, there is a switch to select between different input signals, namely 1) the noise injection signal for the CAS measurement, 2) the antenna signal, 3) the matched load (U- or Dicke load), and 4) the CAS signal.

In order to prevent cross coupling of a noise injected into the other receiver channel over antenna (this would give an offset to the measurement of the third and fourth Stokes parameters), an isolation requirement of 43 dB was set for the coupler; at the same time, transmission loss and physical size should be minimized. No space-qualified coupler could be found with sufficiently high performance. Therefore, a custom coupler was developed within this project.

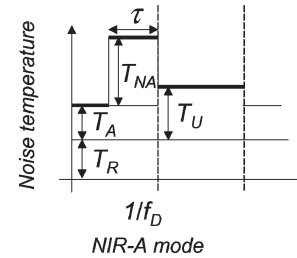


Fig. 4. Schematic diagram of the power detector output in the NIR-A mode. One Dicke cycle is the period  $1/f_D$  and  $\tau$  is the length of a constant amplitude noise injection pulse expressed as a fraction of the half of the Dicke cycle;  $T_R$  is the receiver noise temperature;  $T_A$  is the antenna brightness temperature;  $T_{NA}$  is the noise injection temperature, and  $T_U$  is the noise temperature of the matched reference load, or Dicke load.

The physical temperature of NIR is not controlled; therefore, a software correction is applied to correct for the small changes of the radiometric response with temperature [10]. See Section III-B4 for details.

### B. Operation of Reference Radiometer

The NIR operates by injecting (or adding) a known and constant amplitude noise temperature pulse to the antenna signal. The level of the combined antenna signal and the injected noise is adjusted to achieve a balance with respect to a reference (or Dicke) load. This adjustment is accomplished by adjusting the length of the pulse. Both Dicke half cycles being balanced, the method removes the effect of the receiver gain and offset variations. The length of the noise injection pulse is then proportional to the antenna temperature [11]. The amount of the injected noise is controlled by the FPGA, i.e., the feedback loop is controlled digitally. The control is based on the calculation of the noise difference between the two Dicke half cycles, and adjusting the change of the noise injection level based on this. One great benefit of this method is the fact that there is practically no possibility of the control loop starting to oscillate. Fig. 4 presents a schematic diagram of the power detector output of one receiver in NIR-A mode; this demonstrates how the noise injection balances the input of the radiometer.

The NIR has several operational modes for measuring the antenna and CAS noise temperature and for calibration. The antenna temperature is measured using a noise injection mode called NIR-A mode and the CAS noise level is measured using a noise injection mode called NIR-R mode. Also, total power modes are used, for example, for solving the receiver noise temperature. Table II lists the operational modes of the NIR. For the measurement of the receiver noise temperature, two modes are used: one has the intermediate frequency (IF) attenuator ON and the other has it OFF in order to apply the so-called four-point method (explained in for example [12]).

The equations for NIR operation are presented in the following two sections. The model for the calibration of the front end of the NIR follows the principle of the theory of the radiative transfer, i.e., [9], [11]

$$T' = \frac{T}{L} + \left(1 - \frac{1}{L}\right) T_{\text{phys}} \quad (3)$$

TABLE II  
OPERATIONAL MODES OF THE NIR (M/C STANDS FOR MEASUREMENT  
MODE OR CALIBRATION MODE)

Mode	M/C	Purpose
NIR-A	M+C	Measurement of antenna temperature, $T_A$ , and calibration of antenna injection, $T_{NA}$
NIR-R	M	Measurement of CAS noise level, $T_{CAS}$
NIR-AR	C	Calibration of reference injection, $T_{NR}$
LICEF-LC	C	Measurement of receiver noise temperature (IF-attenuator OFF), $T_{rec}$ , and receiver phase imbalance $\Theta_{rec}$
LICEF-LC2	C	Measurement of receiver noise temperature (IF-attenuator ON), $T_{rec}$
LICEF-LU	C	Measurement of residual offset, $V_U$
LICEF-LA	C	Measurement of Corbella correlation, $V_C$

where  $T$  is the input noise temperature of a passive network,  $T'$  is the output noise temperature,  $T_{phys}$  is the physical temperature of the loss  $L$ , which is the loss causing the equivalent noise temperature of the passive network. This is defined at the input of the network as [11], [13], [14]

$$T_e = (L - 1)T_{phys} = \left( \frac{1 - |S_{22}|^2}{|S_{21}|^2} - 1 \right) T_{phys} \quad (4)$$

where  $S$  refers to the scattering parameters of the network. This yields for the relation between the loss parameter and the scattering parameters

$$L = \frac{1 - |S_{22}|^2}{|S_{21}|^2}. \quad (5)$$

This definition is used for the loss  $L$  in the subsequent sections (as opposed to using  $S_{21}$  directly) in order to take the matching of the components into account.

In order to solve the antenna temperature, the front end and the antenna is divided in sections, as shown in Fig. 3. This is done to account for the facts that the noise injection level  $T_{NA}$  needs to be determined in the calibration, and that the controller, cables, and receivers are located in different thermal environments, as can be seen in Fig. 1. The equations are derived in a way similar to the ones for the prototype presented in [5].

1) *Antenna Measurement*: The NIR is calibrated by solving the calibration parameters  $A$  and  $B$  in order to solve the antenna temperature from the following equation:

$$T_A = A\tau_A + B. \quad (6)$$

The parameter  $A$  is defined as

$$A = -L_1 L_2 T_{NA} \quad (7)$$

where  $L_1$  is the loss of the antenna patch and  $L_2$  is the loss of the intermediate layer of the antenna. The parameter  $B$  is defined as

$$B = L_1 L_2 (L_{NC} L_A L_{DA} (T_{pU} - T_{t2}) - T_{t1}) \quad (8)$$

where  $L_{NC}$  is the insertion loss of the coupler (including the connections inside the NIR Controller);  $L_A$  is the loss of the

cable between the coupler and the receiver;  $L_{DA}$  is the loss of the Dicke switch;  $T_{pU}$  is the physical temperature of the internal reference load;  $T_{t2}$  is the thermal noise of the path from the coupler to the output of the Dicke switch and  $T_{t1}$  is the thermal noise of the antenna defined as follows:

$$T_{t1} = \left(1 - \frac{1}{L_1}\right) \frac{T_{p7}}{L_2} + \left(1 - \frac{1}{L_2}\right) T_{p6} \quad (9)$$

where  $T_{p7}$  is the physical temperature of the antenna patch and  $T_{p6}$  is the physical temperature of the intermediate layer of the antenna, and

$$T_{t2} = \left(1 - \frac{1}{L_{NC}}\right) \frac{T_{p3}}{L_A L_{DA}} + \left(1 - \frac{1}{L_A}\right) \frac{T_{cab}}{L_{DA}} + \left(1 - \frac{1}{L_{DA}}\right) T_{pU} \quad (10)$$

where  $T_{p3}$  is the physical temperature of the coupler and  $T_{cab}$  is the physical temperature of the cable between the coupler and the receiver approximated with

$$T_{cab} = \frac{T_{p3} + T_{pU}}{2}. \quad (11)$$

The level of the noise injection is determined by measuring a known target,  $T_{A0}$ , which is the cold sky in the case of the NIR, yielding

$$T_{NA} = \frac{1}{L_1 L_2} \left( \frac{B - T_{A0}}{\tau_A} \right). \quad (12)$$

The third and fourth Stokes parameters are solved using the following equation:

$$T_3 = 2\sqrt{\hat{T}_{Av}\hat{T}_{Ah}} \Re\{\tilde{V}\} \quad (13)$$

$$T_4 = 2\sqrt{\hat{T}_{Av}\hat{T}_{Ah}} \Im\{\tilde{V}\} \quad (14)$$

where  $\hat{T}_{Av}$  and  $\hat{T}_{Ah}$  are linearity corrected (see Section III-B) vertical and horizontal antenna brightness temperatures and  $\tilde{V}$  is the amplitude-corrected (the effect of the receiver noise removed) correlation coefficient. See [5] for details of the amplitude correction in the case of the NIR.

2) *CAS Measurement*: CAS measurement is calibrated by determining the calibration parameters  $A_R$  and  $B_R$ . The CAS output noise temperature is solved as follows:

$$T_{CAS} = A_R \tau_R + B_R \quad (15)$$

where  $\tau_R$  is the length of the noise injection in the CAS measurement mode (NIR-R mode). The calibration parameter  $A_R$  is written as

$$A_R = \frac{T_{NR} L_{DC}}{L_R L_{DR}} \quad (16)$$

where  $T_{NR}$  is the level of the noise injection;  $L_{DC}$  and  $L_{DR}$  are the loss of the Dicke switch in CAS measurement and noise injection positions, respectively, and  $L_R$  is the loss of the cable

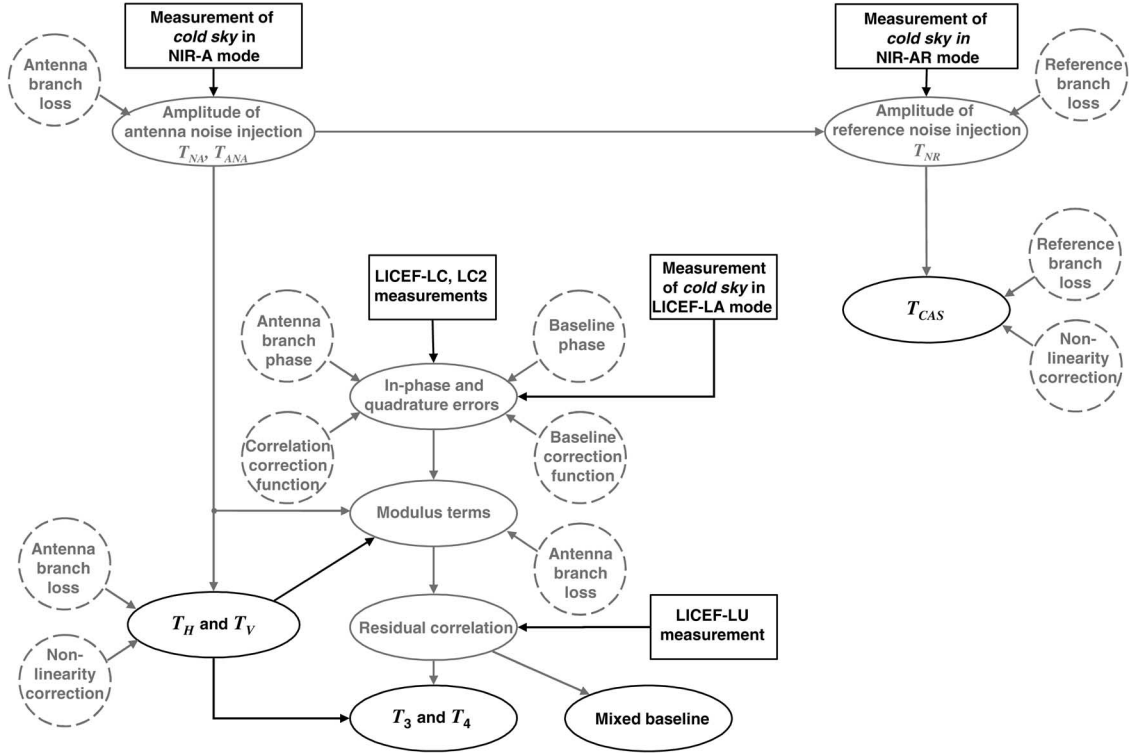


Fig. 5. Calibration flow of the reference radiometer. The black rectangles depict measurements, gray ellipses depict the solving of intermediate parameters, black ellipses depict the solving of the end products, and the gray circles with dashed lines depict the application of the ground calibration values. Certain operational modes are mentioned in the black rectangles; NIR-A mode for solving the noise injection level for antenna measurement (and for solving antenna temperature), NIR-AR mode for solving the noise injection level for CAS measurement, LICEF-LC and LICEF-LC2 modes for measuring the CAS so that the IF-attenuator of the receiver is OFF and ON, respectively, LICEF-LA for measuring the antenna temperature in total power mode and LICEF-LU for measuring the uncorrelated load.

through which the noise is injected. The calibration parameter  $B_R$  is written as

$$B_R = \frac{T_{p3}}{L_R} \frac{L_{DC}}{L_{DR}} + T_{t3} \quad (17)$$

where  $T_{p3}$  is the physical temperature of the reference load used in the NIR-R mode and

$$T_{t3} = \left(1 - \frac{1}{L_R}\right) \frac{L_{DC}}{L_{DR}} T_{cab} + \left(1 - \frac{L_{DC}}{L_{DR}}\right) T_{pU}. \quad (18)$$

The noise injection level is determined by measuring a known target, cold sky in the case of the NIR, in the so-called NIR-AR mode, which can be formulated as

$$T_{NR} = \frac{L_R L_{DR}}{\tau_{AR}} \left( T_{ANA} - \frac{T_{p3}}{L_R L_{DR}} - T_{t3} \right) \quad (19)$$

where  $T_{ANA}$  is the noise level in the antenna channel during noise injection and  $\tau_{AR}$  is the length of the noise injection in the NIR-AR mode.

### III. CALIBRATION OF REFERENCE RADIOMETER

#### A. Calibration Approach

The calibration approach for the reference radiometer includes two steps; 1) certain parameters are characterized on

the ground and 2) these parameters are applied during orbital calibration, which is carried out frequently. The orbital calibration is based on the measurement of the cold sky, which has a well-known brightness temperature level. The cold sky is measured during the external calibration procedure of the SMOS, in which the entire satellite is pointed to the cold sky for a period of about half an orbit. Fig. 5 shows a block diagram of the orbital calibration of the NIR. In the figure, black rectangles depict measurements in the various modes of the targets. The key measurements (cold sky in the NIR-A and NIR-AR modes) are shown at the top of Fig. 5. These measurements are made in order to determine the noise injection levels  $T_{NA}$  and  $T_{NR}$ . This process involves ground calibration parameters, which are depicted in the figure with gray circles with dashed lines. The black ellipses indicate the solving of the end products: fully polarimetric antenna temperature, CAS noise level and correlations for the mixed baselines (which are not discussed in detail in this paper). These steps also include the application of ground calibration parameters.

Furthermore, there are measurements in the LICEF-LC and -LC2 modes, which measure the two levels of CAS (with IF-attenuator OFF and ON, respectively, in order to apply the four-point method) for the receiver noise temperature and phase imbalance measurements. The measurement of the cold sky is also performed in the LICEF-LA mode. This is for determining the so-called Corbella correlation, which is due to the finite isolation between the channels over antenna [15]. Finally, there

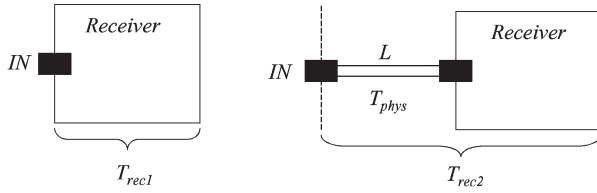


Fig. 6. Principle for solving the loss of the front-end connections of the radiometer.

is a measurement in LICEF-LU mode, in which both channels of the NIR measure the matched loads, also known as the Dicke loads or uncorrelated loads, inside the receivers, in order to determine the residual correlation offset. Each of these steps also include the application of the ground calibration parameters.

The following parameters were solved during the on-ground characterization: 1) antenna and front-end loss, 2) the phase imbalance between V- and H-channels (or V-H phase imbalance) of the antenna and front end, 3) nonlinearity correction, and 4) the temperature dependence of the noise injection level. These parameters are applied during orbital calibration when the level of the noise injection, receiver noise temperature and V-H phase imbalance of the channels are solved. After this, the correction for the nonlinearity is applied to the measured level of brightness temperature. The calibration of the mixed baselines is out of the scope of this paper.

### B. Ground Characterization Principles

1) *Loss Parameters*: In order to solve the loss of the different sections of the front end, the receiver noise temperature is measured in two planes; in the incoming plane and in the outgoing plane of this particular section of the front end. See Fig. 6 for clarification.

For the measurement of the receiver noise temperature, ambient and cold loads are used; either matched coaxial loads or reference antenna targets, depending on the type of the section under study. The return loss of the coaxial loads is measured to be over 30 dB. The cold coaxial load is cooled down with liquid nitrogen and the temperature distribution in the connecting cable is measured and compensated for using the loss of the cable [10]. The return loss of the antenna targets is estimated to be better than 30 dB, based on the reflection coefficient of the applied absorber material (with 25-cm pyramids), which is specified to be 35 dB at the frequency band.

The loss is solved as follows using the definition for the equivalent noise temperature and receiver noise temperature [11]:

$$T_{rec2} = T_e + LT_{rec1} = (L - 1)T_{phys} + T_{rec1} \quad (20)$$

yielding

$$L = \frac{T_{rec2} + T_{phys}}{T_{rec1} + T_{phys}} \quad (21)$$

where  $L$  is the loss,  $T_{rec2}$  and  $T_{rec1}$  are the receiver noise temperatures with and without the loss in front of the receiver, respectively, and  $T_{phys}$  is the physical temperature of the loss element.

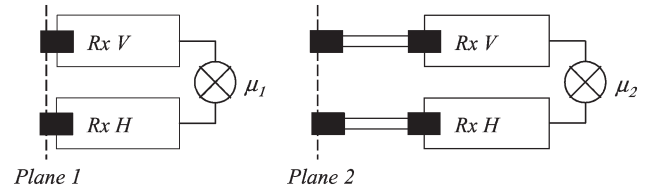


Fig. 7. Principle for solving the V-H phase imbalance between plane 1 and plane 2 is based on measuring a correlated source connected to these planes.

2) *Phase Parameters*: Two separate setups are needed for solving the V-H phase imbalance of the front end and the antenna. The difference of the phases of the correlations measured with the two setups yields the V-H phase imbalance of the front end. See Fig. 7 for clarification. The V-H phase imbalance of the section in front of the receivers can be solved as

$$\Delta\Theta = \arg(\mu_2) - \arg(\mu_1) \quad (22)$$

where  $\Delta\Theta$  is the V-H phase imbalance of the front-end section (between plane 1 and plane 2), and  $\mu_2$  and  $\mu_1$  are the correlations measured with and without the front-end section, respectively. Note that, in order for this formulation to work, either the correlations  $\mu_1$  and  $\mu_2$  have to be measured using the same source or the correlations have to be in-phase calibrated (see, for example, [5]).

A correlated noise source connected to the two receivers of the radiometer can be used for the measurement when the antenna is not included. However, when the antenna is included, the measurement of the V-H phase imbalance on this plane is more complicated. The so-called dual-angle method can be used for this [16]. The idea of this method is to measure linearly polarized correlated noise at two different angles, which are at 90° separation and at a 45° angle with respect to the polarization plane of the antenna of the radiometer. The method comes down to the following equation:

$$\Theta = \arctan\left(\frac{\Im\{M_{-45}\} - \Im\{M_{+45}\}}{\Re\{M_{-45}\} - \Re\{M_{+45}\}}\right) \quad (23)$$

where  $\Theta$  is the V-H phase imbalance and  $M_{-45}$  and  $M_{+45}$  are the quadrature-corrected (see, for example, [5]) correlations obtained at  $-45^\circ$  and  $+45^\circ$  angles with respect to the electric field of the transmitted field, respectively.

3) *Nonlinearity Correction*: There are two sources of error that are taken into account in the so-called nonlinearity correction. The first is the nonlinearity of the detector of the receiver and the second is the fact that the coupling of the directional coupler is assumed to be an ideal adder in the equations of operation. To this end, the technique presented in [17], and modified by Vilaseca from Mier Comunicaciones, Spain, [18] is applied here to the case of a NIR.

Fig. 8 shows a schematic diagram of the measurement setup used in this technique. The idea is to add a constant amount of noise on top of a noise level that can be varied. The benefit of this method is the fact that the only critical parameter for the accuracy of the measurement is the stability of the added noise, which is achieved relatively easily.

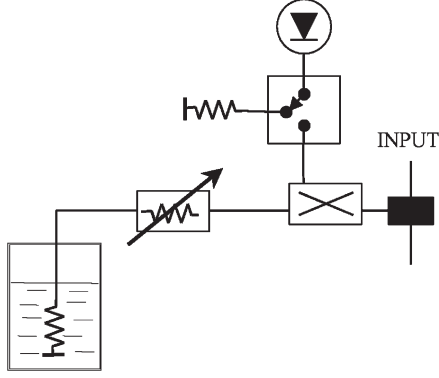


Fig. 8. Setup for measuring the nonlinearity. The noise from the noise diode is added on top of the noise coming from the cold load cooled with liquid nitrogen. The noise level from the cold load can be varied using the controllable attenuator.

The linear and quadratic correction is applied to the antenna temperature as follows:

$$\hat{T}_A = T_A + T_{\text{lin}} \quad (24)$$

where  $\hat{T}_A$  is the corrected antenna temperature,  $T_A$  is the antenna temperature before the correction is applied, and

$$T_{\text{lin}} = c(T_A - T_0) + d(T_A - T_0)^2 \quad (25)$$

in which  $c$  is the linear correction term,  $d$  is the quadratic term and  $T_0$  is the antenna temperature during calibration.

Using (6) and (25), the length of noise injection can be written as

$$\tau^{\text{OFF}} = \left[ \hat{T}_A - B - c(T_A - T_0) - d(T_A - T_0)^2 \right] \frac{1}{A} \quad (26)$$

where  $\tau^{\text{OFF}}$  is the length of the noise injection when the additional noise is OFF. When the additional noise is on the length of the noise injection is written as

$$\tau^{\text{ON}} = \left[ \hat{T}_A - B - c(T_A + \Delta T - T_0) - d(T_A + \Delta T - T_0)^2 \right] \frac{1}{A} \quad (27)$$

in which  $\Delta T$  is the amount of the additional noise.

Now, the difference between the situations when the noise injection is OFF and ON can be solved. This equation allows us to write the difference in the form of a straight line

$$\Delta\tau = \tau^{\text{OFF}} - \tau^{\text{ON}} \quad (28)$$

$$= \frac{2d\Delta T}{A}(T_A - T_0) + \frac{1}{A}(d\Delta T + c - 1) \quad (29)$$

$$= k_1(T_A - T_0) + k_2 \quad (30)$$

where  $k_1$  and  $k_2$  are the slope and offset of the line, respectively. Now, using these coefficients the parameters  $c$  and  $d$  can be solved

$$c = \frac{A}{\Delta T} k_2 - d\Delta T + 1 \quad (31)$$

and

$$d = \frac{1}{2} \frac{A}{\Delta T} k_1. \quad (32)$$

The slope of the line  $k_1$  determines the quadratic term, and parameters  $k_1$  and  $k_2$  together determine the linear term. Note that  $A$  is actually the level of the noise injection, and that its changes cause only second-order uncertainty to the correction. A similar set of equations is derived for the CAS measurement.

4) *Temperature Dependency of Noise Injection*: A study of the temperature sensitivity of the reference radiometer's prototype is presented in [10]. Some results for the engineering model are presented in [19]. The results showed that the fit of a linear correction model to the data points was very good (i.e., low scatter and good repeatability). The applied linear model accounts also for all the changes of loss and matching of every component correcting the fixed-loss model. Several correction models (with respect to the fixed-loss model) were studied with the prototype [10], which took the temperature changes of different components into account independently. The results showed that the model based only on the temperature of the noise source was as accurate as the models based on several measured temperatures.

The correction model is acquired by measuring a known noise source connected to the antenna output plane (which excludes the antenna from the measurement) while the physical temperature of the NIR is cycled. Additionally, the effect of the antenna and its connection is modeled in orbit during the commissioning phase of the mission. However, their effect is expected to be very small, or even negligible.

## IV. GROUND CALIBRATION RESULTS

### A. Antenna and Front-End Loss

Table III lists the loss parameters of the antenna and the connection between the antenna output planes and the input planes of the LICEF-units. For comparison, the loss was also measured with a vector network analyzer (VNA), also shown in Table III. The accuracy of the VNA measurement is specified to be 0.05 dB for normal range measurements, but for this kind of low-loss measurements it is worse than that; however, the accuracy of the radiometric characterization measurement is in the order of 0.01 dB. However, the results of Table III show very similar values (within 0.02 dB) for every other channel except H-channel of NIR-3 (0.06 dB). The result shows that the radiometric measurement also accounts for the matching of the front end, which is critical.

In general, the front-end losses show very similar results for the V- and H-channels; the only exception is NIR-3, which shows a small (0.10 dB) difference. A potential explanation

TABLE III  
LOSS OF THE FRONT-END CONNECTIONS AND ANTENNAS DERIVED WITH RADIOMETRIC MEASUREMENT AND ALSO LOSS OF THE FRONT-END CONNECTIONS DERIVED FROM S-PARAMETERS

	$S_{21}^{NC}$ [dB]	$S_{22}^{NC}$ [dB]	$S_{21}^A$ [dB]	$S_{22}^A$ [dB]	$L_S^1$ [dB]	$L_C^2$ [dB]	$L_{ant}^3$ [dB]
NIR-1 V	-0.28	-18.8	-0.16	-29	0.38	0.38	0.20
NIR-1 H	-0.24	-19.2	-0.16	-29	0.34	0.36	0.17
NIR-2 V	-0.27	-19.4	-0.16	-29	0.37	0.35	0.17
NIR-2 H	-0.30	-18.0	-0.16	-29	0.38	0.36	0.12
NIR-3 V	-0.32	-17.0	-0.16	-29	0.38	0.38	0.12
NIR-3 H	-0.32	-18.3	-0.16	-29	0.42	0.48	0.16

- 1) Front-end loss ( $L_S = L_S^{NC} + L_S^A$ ) determined using Eqn (5).
- 2) Front-end loss ( $L_C = L_{NC} + L_A$ ) determined in one piece using the radiometric measurement (Section III-B.1).
- 3) Antenna loss ( $L_{ant} = L_1 + L_2$ ).

TABLE IV  
V-H PHASE IMBALANCE (FOR NOMINAL AND REDUNDANT CORRELATIONS) OF THE ANTENNAS AND THE FRONT-END CONNECTIONS

	Receiver Plane Nominal (Redundant) $\Theta_{rec}$ [deg]	Antenna Plane Nominal (Redundant) $\Theta$ [deg]	Difference Nominal (Redundant) $\Delta\Theta$ [deg]
NIR-1	-49.7 (-49.3)	-38.0 (-37.6)	11.7 (11.7)
NIR-2	-49.3 (-48.3)	-41.9 (-40.3)	7.4 (8.0)
NIR-3	-29.1 (-30.2)	-11.1 (-11.3)	18.0 (18.9)

for the loss imbalance of NIR-3 is the manufacturing process, which includes many manual steps. These are prone to small variations, which can lead to imbalance if summed up.

B. Antenna and Front-End Phase Imbalance

Table IV shows the V-H phase imbalance of the front end (between antenna output plane and input plane of LICEF-units) and of the antenna for nominal and redundant correlations. For comparison, the V-H phase imbalance of the front end was also measured with a VNA showing very similar results. However, the phase measurement accuracy of the VNA measurement is worse than the accuracy of the characterization measurement that uses correlations.

The results for NIR-1 and NIR-2 V-H phase imbalance are relatively equal, but the result for NIR-3 is different. A potential explanation lies in the manual manufacturing processes, as was the case in the front-end loss differences. The fact that the loss imbalance in NIR-3 is significant can explain the different V-H phase imbalance as well.

C. Nonlinearity Correction

Table V presents the nonlinearity correction parameters for all three NIR units. V- and H-channels have a systematic difference, which is explained by the different layout of the channels. Fig. 9 shows the nonlinearity correction for V- and H-channels of NIR-1 as an example. A calibration target of about 120 K, which is the output noise temperature of the

TABLE V  
NONLINEARITY CORRECTION FOR THE ANTENNA MEASUREMENT

	$c$ ( $10^{-3}$ )	$d$ ( $10^{-5}$ )
NIR-1 V	4.69	-2.74
NIR-1 H	7.29	-4.28
NIR-2 V	4.30	-2.47
NIR-2 H	10.4	-6.09
NIR-3 V	4.86	-2.92
NIR-3 H	8.34	-5.01

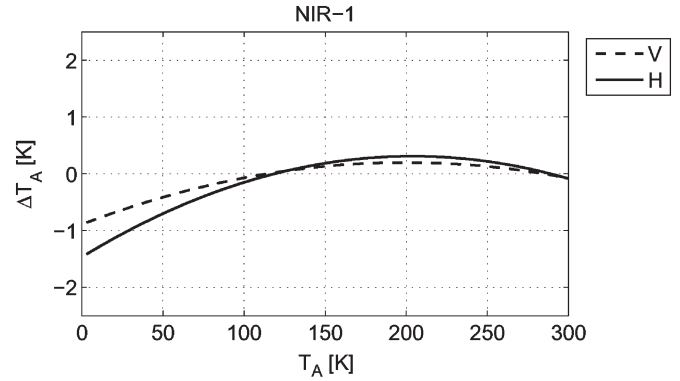


Fig. 9. Nonlinearity correction of NIR-1 for V- and H-channels.

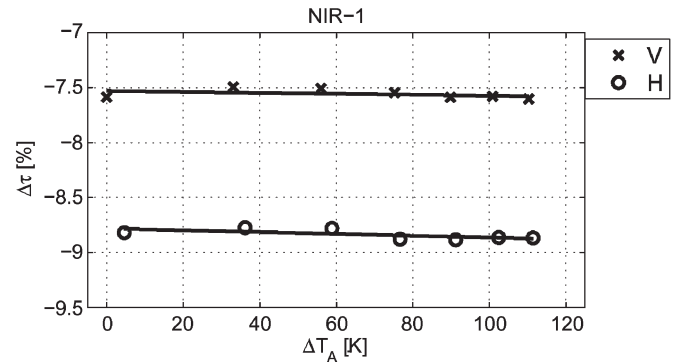


Fig. 10. Coefficients for the nonlinearity correction is solved by fitting the lines, defined by  $k_1$  and  $k_2$ , to the measurement points as in this figure.

coaxial reference load used in the measurement, is assumed. The correction is, at maximum only slightly over 1 K, V- and H-channels having very similar curves.

Fig. 10 shows examples of the fitted lines of (28) with slope of  $k_1$  and offset of  $k_2$  for V- and H-channels of NIR-1. The deviations from the line are small, indicating the reliability of the method.

D. Temperature Dependency of Noise Injection

The thermal cycling consisted of at least two cycles ranging from +10 °C to +40 °C, which is the operational range of the subsystem, for each unit. The results showed that the temperature dependence of the antenna and reference noise injection of both channels of all units is under 0.1%/°C. Due to the fact that the noise injection length (expressed as a fraction of the half of the Dicke cycle) is typically 10% to 40%, the effect of the noise injection variation on the measured antenna temperature is in

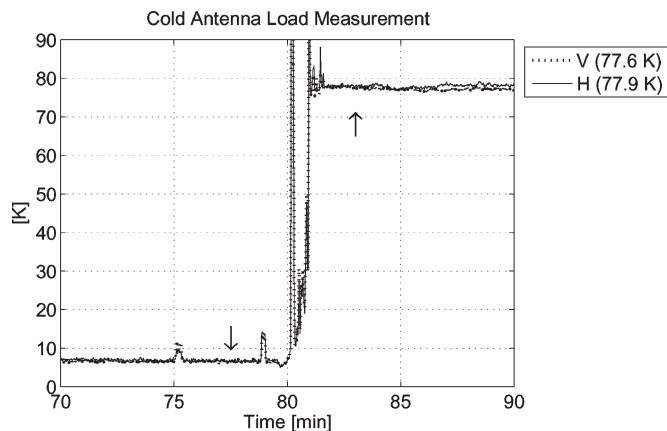


Fig. 11. Result of the calibration experiment performed with the engineering model. The down arrow shows the calibration epoch and the up arrow shows the epoch during which the cold load temperature is determined.

the order of  $0.025\%/^{\circ}\text{C}$ . This can be reduced further by a factor of 5 to 10 using the linear model for the variation of the noise injection level with temperature.

Furthermore, it is important to note that the temperature variation in the orbit is expected to be less than the operational range. Based on the payload level thermodynamical simulations carried out by EADS-CASA Espacio, Spain, the thermal variation of the antenna patch, during one orbit, is around  $15^{\circ}\text{C}$ , that of the controller and the intermediate layer of the antenna is around  $2^{\circ}\text{C}$  and that of the LICEF units is around  $1^{\circ}\text{C}$ . Also, the thermal gradient is expected to be very constant between the different components.

#### E. Calibration Experiment With Engineering Model

An experiment to validate the calibration approach was conducted with the engineering model using the sky and a cold antenna target as references. During the experiment sky was clear, and the sun in the horizon. The cold target was an absorber load cooled down with liquid nitrogen.

First, the calibration was performed by a measurement of the sky, and then the cold load was measured in order to compare the measurement result to the predicted brightness temperature. During the experiment, the temperature of the NIR varied strongly, and also the gradient between the components changed dramatically, which is not representative for the in-orbit case. For this reason, a dedicated thermal model was used in the analysis of the results.

Fig. 11 shows the results of the experiment for both V- and H-channels. The down arrow shows the calibration epoch and the up arrow shows the epoch during which the cold load temperature is determined. The jumps in the plot are due to the positioning of the radiometer. The obtained cold load values are 77.6 K for the V-channel and 77.9 K for the H-channel. These values correspond well to the predicted values, as the brightness temperature of sky is assumed to be 6.6 K and the temperature of the liquid nitrogen is 77.35 K. This result shows that the concept of the calibration, i.e., one reference target with characterization of the front end, works.

TABLE VI  
SUMMARY OF PERFORMANCE PARAMETERS OF NIR

	NIR-1	NIR-2	NIR-3
Receiver noise $V$	259 K	248 K	260 K
Receiver noise $H$	260 K	262 K	252 K
Resolution $V$	0.19 K	0.20 K	0.24 K
Resolution $H$	0.22 K	0.24 K	0.24 K
Resolution 3	0.43 K	0.41 K	0.45 K
Resolution 4	0.43 K	0.49 K	0.41 K
Stability $V^1$	0.086 K/ $^{\circ}\text{C}$	0.007 K/ $^{\circ}\text{C}$	0.043 K/ $^{\circ}\text{C}$
Stability $H^1$	0.066 K/ $^{\circ}\text{C}$	0.007 K/ $^{\circ}\text{C}$	0.040 K/ $^{\circ}\text{C}$
Channel isolation	>100 dB	>100 dB	>100 dB
Coupler <sup>2</sup> :			
Insertion loss $V / H$	0.16 dB / 0.16 dB		
Isolation $V / H$	50 dB / 45 dB		

1) With the compensation in the operational range from  $+10^{\circ}\text{C}$  to  $+40^{\circ}\text{C}$ .

2) Measured from samples of the same manufacturing lot.

#### V. PERFORMANCE SUMMARY

Table VI summarizes the performance of NIR FM. The noise temperature and radiometric resolution values are within the requirements in all cases. Also, the design of the coupler was very successful; very high isolation could be combined with extremely low loss and small size ( $10 \times 10 \times 1.3$  mm). Furthermore, the isolation between orthogonal channels (vertical and horizontal) is very high. Note, however, that the presented figure does not include the cross-coupling of the antenna.

The stability as a function of the physical temperature does not satisfy the requirement in the cases of NIR-1 and NIR-3. However, the presented values are estimates and the measurement situation was not entirely representative. Furthermore, in the measurement the units were cycled between  $10^{\circ}\text{C}$  to  $40^{\circ}\text{C}$  relatively rapidly; in the orbit the thermal fluctuation of the units is, based on the simulations, around  $2^{\circ}\text{C}$  per orbit (excluding antenna patch surface, which experiences greater excursion). Thus, the performance is considered satisfying in this respect also.

#### VI. CONCLUSION

The FMs of the NIR subsystem (reference radiometers) of SMOS have been designed, manufactured, tested, and characterized. The key performance parameters were retrieved, a ground calibration campaign was conducted and the units passed the environmental acceptance and qualification tests. In most cases, the measured performance parameters met the original requirements set for the NIR subsystem of SMOS. The only exception was the stability with varying physical temperature; it proved to be challenging to fulfill this stringent requirement under the budgetary and schedule constraints of the project. However, the modeling of the behavior with temperature and the application of software correction improve the stability. The retrieved ground calibration results will be used for the in-orbit calibration of the NIR and MIRAS. The in-orbit calibration was also designed to include the appropriate steps to fulfill the measurement purposes of the NIR.

## ACKNOWLEDGMENT

The authors would like to thank the following individuals for their assistance: P. Rummukainen and K. Forsberg from TKK, P. Ketola, E. Kivinen, M. Koski, I. Lehtikainen, S. Nevalainen, K. Nyqvist, H. Putkinen, and S. Lotvonen from Elektrobitt, Ltd., M. Mäkelä from the Finnish Meteorological Institute, M. Bergadá and A. Solana from EADS-CASA Espacio, and Dr. M. Martín-Neira from ESA/ESTEC.

## REFERENCES

- [1] T. Schmugge, P. E. O'Neill, and J. R. Wang, "Passive microwave soil moisture research," *IEEE Trans. Geosci. Remote Sens.*, vol. GRS-24, no. 1, pp. 12–22, Jan. 1986.
- [2] H.-J. C. Blume, B. M. Kendall, and J. C. Fedors, "Measurement of ocean temperature and salinity via microwave radiometry," *Boundary-Layer Meteorol.*, vol. 13, no. 1, pp. 295–308, Jan. 1978.
- [3] P. Silvestrin, M. Berger, Y. Kerr, and J. Font, "ESA's second earth explorer opportunity mission: The soil moisture and ocean salinity mission—SMOS," *IEEE Geosci. Remote Sens. Newsl.*, no. 118, pp. 11–14, Mar. 2001.
- [4] J. Lahtinen, L. Ruokokoski, A. Colliander, V. Kangas, A. Aalto, M. Levander, and H. Greus, "Reference radiometer for interferometric radiometry from space," in *Proc. IEEE IGARSS*, Seoul, South Korea, 2005, pp. 5551–5553.
- [5] A. Colliander, S. Tauriainen, T. I. Auer, J. Kainulainen, J. Uusitalo, M. Toikka, and M. T. Hallikainen, "MIRAS reference radiometer: A fully polarimetric noise injection radiometer," *IEEE Trans. Geosci. Remote Sens.*, vol. 43, no. 5, pp. 1135–1143, May 2005.
- [6] M. Martín-Neira and J. M. Goutoule, "A two-dimensional aperture-synthesis radiometer for soil moisture and ocean salinity observations," *ESA Bull.*, no. 92, pp. 95–104, Nov. 1997.
- [7] I. Corbella, F. Torres, A. Camps, A. Colliander, M. Martín-Neira, S. Rib, K. Rautiainen, N. Duffo, and M. Vall-llossera, "MIRAS end-to-end calibration. Application to SMOS L1 processor," *IEEE Trans. Geosci. Remote Sens.*, vol. 43, no. 5, pp. 1126–1134, May 2005.
- [8] J. Lemmetyinen, J. Uusitalo, K. Rautiainen, J. Kainulainen, N. Fabritius, M. Levander, V. Kangas, H. Greus, J. Pihlflyckt, A. Kontu, S. Kempainen, M. Hallikainen, and J. Lahtinen, "SMOS calibration subsystem," in *Proc. IEEE IGARSS*, Denver, CO, 2006, pp. 2309–2312.
- [9] L. Tsang, J. A. Kong, and R. T. Shin, *Theory of Microwave Remote Sensing*. New York: Wiley, 1999.
- [10] A. Colliander, S. Tauriainen, T. Auer, J. Uusitalo, M. Toikka, and M. T. Hallikainen, "Evaluation of in-orbit temperature variation on performance of MIRAS prototype noise injection radiometer," in *Proc. IEEE IGARSS*, Anchorage, AK, 2004, pp. 781–784.
- [11] F. Ulaby, R. Moore, and A. Fung, *Microwave Remote Sensing, Active and Passive*, vol. 1. Reading, MA: Addison-Wesley, 1981.
- [12] F. Torres, N. Duffo, I. Corbella, A. Camps, M. Vall-llossera, and S. Ribó, "MIRAS-SMOS: The relative instrumental error calibration approach," in *Proc. 8th Specialist Meeting MicroRad*, Rome, Italy, 2004.
- [13] I. Corbella, F. Torres, A. Camps, N. Duffo, M. Vall-llossera, K. Rautiainen, M. Martín-Neira, and A. Colliander, "Analysis of correlation and total power radiometer front-ends using noise waves," *IEEE Trans. Geosci. Remote Sens.*, vol. 43, no. 11, pp. 2452–2459, Nov. 2005.
- [14] S. W. Wedge and D. B. Rutledge, "Wave techniques for noise modeling and measurement," *IEEE Trans. Microw. Theory Tech.*, vol. 40, no. 11, pp. 2004–2012, Nov. 1992.
- [15] I. Corbella, N. Duffo, M. Vall-llossera, A. Camps, and F. Torres, "The visibility function in interferometric aperture synthesis radiometry," *IEEE Trans. Geosci. Remote Sens.*, vol. 42, no. 8, pp. 1677–1682, Aug. 2004.
- [16] A. Colliander, J. Kettunen, and M. Hallikainen, "Calibration of end-to-end phase imbalance of polarimetric radiometer," *IEEE Trans. Geosci. Remote Sens.*, vol. 44, no. 10, pp. 2635–2641, Oct. 2006.
- [17] N. Skou, "Microwave radiometer linearity measured by simple means," in *Proc. IEEE IGARSS*, Toronto, ON, Canada, 2002, pp. 3664–3667.
- [18] R. Vilaseca, "PMS linearity setup improvement," Mier Comunicaciones, Barcelona, Spain, Project report: SMOS PLM Phase C/D - LICEF 3, SO-RP-MIER-LIC-0233-02, Jun. 20, 2005.
- [19] A. Colliander, J. Suomela, L. Ruokokoski, V. Kangas, A. Aalto, J. Lahtinen, and M. Hallikainen, "Temperature variation compensation in engineering model of MIRAS reference radiometer," in *Proc. IEEE IGARSS*, Seoul, South Korea, 2005, pp. 5558–5561.



**Andreas Colliander** (S'04–A'06) was born in Imatra, Finland, in 1976. He received the M.Sc. (Tech.) and Lic.Sc. (Tech) degrees from the Helsinki University of Technology (TKK), Espoo, Finland, in 2002 and 2005, respectively. He is currently working toward the D.Sc. (Tech) degree in the Laboratory of Space Technology, TKK.

He is currently with the European Space Research and Technology Centre, European Space Agency, Noordwijk, The Netherlands, as Research Fellow. From 2001 to 2007, he was with the Laboratory of Space Technology, TKK, where he was a Research Scientist and Project Manager. His tasks included project management of SMOS NIR, Phase B/C/D, at TKK. From 2003 to 2006, he held a Research Student position at the National Graduate School for Remote Sensing, which was supported by the Finnish Ministry of Education and the Academy of Finland. He has authored or coauthored more than 20 scientific publications on microwave remote sensing. His research interests include microwave radiometry, with emphasis on polarimetric and interferometric radiometer systems, and on theoretical simulation of rough-surface backscattering.

Mr. Colliander was a recipient of the TKK Master's Thesis Award, which is an annual award for top five Master's thesis of TKK.

**Lasse Ruokokoski** received the M.Sc. (Tech.) degree from the Helsinki University of Technology, Espoo, Finland, in 2003. He is currently working toward the M.Sc. (Economics and Business Administration) degree at the Turku School of Economics, Turku, Finland.

From 2001 to 2006, he was with Elektrobitt Microwave (EBM), Ltd., holding the position of Chief Designer and Project Manager. His Master's research focused on active calibration for spaceborne synthetic aperture radars. From 2003 to 2006, he was Elektrobitt Microwave's Chief Designer for L-band noise injection radiometer (NIR) subsystem for the European Space Agency's (ESA) soil moisture and ocean salinity (SMOS) mission.



**Jani Suomela** received the M.Sc. (Tech.) degree from the Helsinki University of Technology (TKK), Espoo, Finland, in 2006.

He is currently a System Engineer with Finavia, the Civil Aviation Administration, Finland. From 2002 to 2006, he was with the Laboratory of Space Technology, TKK, working on the testing and characterization of the reference radiometer of ESA's SMOS mission, design of an airborne L-band polarimetric radiometer, and simulation of microwave scattering from snow and water. He has coauthored

four scientific publications on microwave remote sensing.



**Katriina Veijola** was born in Helsinki, Finland, in 1976. She is currently working toward the M.Sc. (Tech.) degree at the Helsinki University of Technology (TKK).

From 2005 to 2006, she was with the Laboratory of Space Technology, TKK, testing the reference radiometers of ESA's SMOS mission.



**Jani Kettunen** was born in Finland, in 1977. He is currently working toward the M.Sc. (Tech.) degree at the Helsinki University of Technology (TKK). His Master's thesis is focused on HUT-2D interferometric *L*-band radiometer antenna parameter characterization.

He is currently an R&D Test Engineer with Vaisala, Ltd., Vaisala Measurement Systems in Finland. From 2002 to 2006, he was with the Laboratory of Space Technology, TKK, working on his Master's thesis subject, and testing and characteriza-

tion of the reference radiometers of ESA's SMOS mission. He has authored or coauthored seven scientific publications on microwave remote sensing.



**Ville Kangas** received the M.Sc. (Tech.) degree from the Helsinki University of Technology, Espoo, Finland, in 2001.

He is currently a Project Manager with Elektrobit, Radio Networks Solutions in Espoo, Finland. From 2003 to 2006, he was with EBM, Ltd., holding the position of Microwave Design Engineer. From 2002 to 2003, he was a Young Graduate Trainee with ESA's European Research and Technology Centre (ESTEC) in Noordwijk, The Netherlands.



**Aleksii Aalto** is currently working toward the M.Sc. (tech.) degree at the Helsinki University of Technology (TKK), Espoo, Finland.

Since 2001, he has been with the Laboratory of Space Technology, TKK, working on control systems for radiometers and microwave measurements in general. His tasks also involved the implementation of the control FPGA of the near-infrared subsystem of SMOS.

**Mikael Levander**, photograph and biography not available at the time of publication.



**Heli Greus** received the B.Sc. (Tech.) degree from the Rovaniemi University of Applied Sciences, Rovaniemi, Finland, in 2000 and the M.Sc. (Tech) degree from the Helsinki University of Technology, Espoo, Finland, in 2007.

From 2000 to autumn 2003, she was with Space Systems Finland, Ltd., where she was a Systems Engineer. From 2004 to autumn 2006, she was with Elektrobit Microwave Ltd., where she was a Microwave Design Engineer; her responsibilities included product assurance management of the Flight

Model development of SMOS NIR and SMOS CAS subsystems. From autumn 2006 to April 2007, she was an RF Design Engineer at Elektrobit, Ltd., Espoo. She is currently with the European Space Research and Technology Centre, European Space Agency, Noordwijk, The Netherlands, as a Product Assurance Engineer. She has authored one and coauthored two scientific publications.



**Martti T. Hallikainen** (M'83-SM'85-F'93) received the Engineering Diploma (M.Sc.) and the Doctor of Technology degrees from the Helsinki University of Technology (TKK), Espoo, Finland, Faculty of Electrical Engineering, in 1971 and 1980, respectively.

Since 1987, he has been a Professor of space technology with TKK. In 1988, he established the TKK Laboratory of Space Technology and serves as its Director. He was a Visiting Scientist in 1993–1994 with the European Union's Joint Research Centre,

Institute for Remote Sensing Applications, in Italy. He was a Postdoctoral Fellow with the University of Kansas Remote Sensing Laboratory from 1981 to 1983. His research interests include development of microwave sensors for airborne and space-borne remote sensing, development of methods to retrieve the characteristics of geophysical targets from satellite and airborne measurements, and cryospheric applications of remote sensing. His team recently completed the HUT-2D airborne interferometric *L*-band radiometer and is currently involved in technical development work and scientific projects concerning the near-future ESA SMOS satellite.

Dr. Hallikainen was awarded an Asla-Fulbright scholarship for graduate studies at the University of Texas at Austin in 1974–1975. He is the recipient of three IEEE Geoscience and Remote Sensing (GRSS) Awards: 1999 Distinguished Achievement Award, IGARSS'96 Interactive Paper Award, and 1994 Outstanding Service Award. He was awarded the IEEE Third Millennium Medal in 2000, and the Microwave Prize for the best paper in the 1992 European Microwave Conference. He is Vice President of the International Union of Radio Science (URSI) since 2005 and he served as Chair of URSI Commission F in 2002–2005. He is the national official member of URSI Commission F since 1988 and he was Chair of the URSI Finnish National Committee in 1997–2005. He is Vice Chair of the Finnish National Committee of COSPAR since 2000. He is a member of the IEEE GRSS Administrative Committee since 1988 and he served as President of IEEE GRSS in 1996–1997. He was General Chair of the IGARSS'91 Symposium and Guest Editor of the Special IGARSS'91 Issue of the IEEE TRANSACTIONS ON GEOSCIENCE AND REMOTE SENSING (TGARS). He was Associate Editor of TGARS in 1992–2002. He served as Chair of the GRSS Nominations Committee in 1999–2006. He was member of the ESA's Earth Science Advisory Committee in 1998–2001. He is a national delegate to the ESA Earth Observation Data Operations Scientific and Technical Advisory Group since 1995. He was Secretary General of the European Association of Remote Sensing Laboratories (EARSeL) in 1989–1993 and Chairman of the Organizing Committee for the EARSeL 1989 General Assembly and Symposium. He has been a member of the EARSeL Council since 1985. He has been a member of the Advisory Committee for the European Microwave Signature Laboratory of the European Union's Joint Research Centre since 1992.



**Janne Lahtinen** (S'98-M'03) received the M.Sc. (Tech.), Lic.Sc. (Tech.), and D.Sc. (Tech.) degrees from the Helsinki University of Technology (TKK), Espoo, Finland, in 1996, 2001, and 2003, respectively.

From 1995 to 2002, he was with the Laboratory of Space Technology, TKK. From 2002 to 2003, he was a Research Fellow at the European Research and Technology Centre, European Space Agency, Noordwijk, The Netherlands. From 2004 to 2006, he was with Elektrobit Microwave, Ltd., Kauniainen,

where he served in various positions, finally as the Manager of Space and Security. From 2006 to 2007, he was the Director of Space at SF-Design Ltd. (Yinen Electronics), Kauniainen, Finland. Since 2007, he has been an independent consultant. His tasks included the project management of SMOS NIR and SMOS CAS, Phase C/D. He has authored and coauthored more than 40 publications in the area of microwave remote sensing and other fields. His research interests include microwave radiometer systems, calibration systems, and spacecraft hardware.

Dr. Lahtinen served as the Secretary of the Finnish National Committee of COSPAR from 1997 to 2002 and as the Secretary of the Space Science Committee, appointed by Finnish Ministry of Education, from 1999 to 2000. From 2006 to 2007, he was an advisor of the Finnish Space Committee. He was welcomed as a Burgen Scholar by Academia Europaea in 2004 and received the Young Scientist Award of the National Convention on Radio Science in 2001 and the third place in the IEEE GRS-S Student Prize Paper Competition in 2000.